(Received 3 October 2024, Accepted 4 November 2024, Scheduled 10 November 2024)

Adaptive Dual-Band Antenna for 5G and ITS Applications with Monopole-to-Broadside Radiation Characteristics

Chinnathambi Murugan* and Thandapani Kavitha

Department of Electronics and Communication Engineering
Vel Tech Rangarajan Dr. Sagunthala R&D Institute of Science and Technology, Chennai, Tamil Nadu 600064, India

ABSTRACT: This study presents an aperture-coupled slot-fed antenna specifically designed to operate in two frequency bands. It functions seamlessly within the 5.2–5.3 GHz and 5.9–6.1 GHz ranges, featuring unique characteristics: emitting monopole radiation at lower frequencies and transitioning to a broadside pattern at higher frequencies. The 5.2–5.3 GHz band is primarily used for high-speed Wi-Fi (IEEE 802.11 standards) and small cells in 5G networks, as well as radar systems. The 5.9–6.1 GHz band supports Intelligent Transportation Systems (ITS), vehicle-to-everything (V2X) communication, and C-band satellite uplink services. With a peak gain of 6.025 dBi, this compact antenna measures $25\,\text{mm} \times 25\,\text{mm} \times 1.6\,\text{mm}$ ($0.492\lambda \times 0.492\lambda \times 0.0315\lambda$, where λ is the wavelength calculated at 5.9 GHz) and is precisely printed on two FR4 substrates, ensuring both performance and practicality. Thorough measurements of the constructed prototype show a remarkable alignment between simulated and measured results, confirming the antenna's reliability and precision. Its distinctiveness lies in its engineered adaptability, perfectly suited for applications requiring diverse patterns within dual-band scenarios. This adaptability allows for flexible signal reception, making it an ideal choice for situations demanding robust performance across multiple frequency ranges. Given its ability to offer varied pattern configurations, this antenna shows significant promise for applications where flexible and reliable signal reception is crucial.

1. INTRODUCTION

The telecommunications industry is rapidly advancing to meet the increasing demand for faster data transfer and wider bandwidth, driven by the widespread use of mobile devices. However, optimizing device performance for data transmission and multimedia applications with minimal delay poses several challenges [1]. A major concern is the management of frequency and equipment allocation in wireless technology, where antennas play a crucial role in supporting technologies like WLAN, 3G, 4G, and the emerging 5G. The growing need for fast and reliable connections is largely fueled by the Internet of Things (IoT), which facilitates communication between wireless devices and the handling of large volumes of data. Although the widespread adoption of 5G is expected by 2025, full standardization is still in progress, with the 3G Partnership Project (3GPP) 5G Release-16 anticipated by 2022 [2–4].

Future 5G systems are expected to offer higher capacity, faster data speeds, low latency, and reliable communication for numerous connected devices [5–7]. Connectivity trends are increasingly focusing on low latency, high user densities, enhanced multimedia services, IoT integration, application convergence, and accurate positioning, as highlighted in multiple studies. Despite 5G's advantages — such as high data rates, low latency transmission, extensive device connectivity, and increased channel capacity — its implementation poses challenges for both Base Transceiver Stations (BTSs) and User Equipment (UE) [8–11]. This generation of wireless technology relies on high-frequency millimeter waves, which offer greater bandwidth than 3G and 4G. Millimeter waves hold significant potential, supporting data transfer speeds and capacities far exceeding those of current cellular networks [12–16].

Designing antennas for 5G networks requires meeting specific criteria, including operation at high frequencies (typically above 24 GHz) and exploring the largely untapped millimeter-wave spectrum (3–300 GHz). Higher frequency bands, such as 24.25–27.5 GHz, 26.5–27.5 GHz, 37–37.6 GHz, and 37.5–42.5 GHz, are actively being employed by various countries for 5G deployment. Antennas must be compact to integrate seamlessly into different infrastructures while maintaining high efficiency and gain to satisfy coverage and capacity needs [17–21]. Achieving optimal performance in the challenging 5G environment requires careful attention to antenna design.

Microstrip antennas, known for their low profile and lightweight nature, are commonly used in wireless communication. However, their low gain can be a limitation in certain applications. Various techniques have been explored to enhance the gain of microstrip antennas. A high-gain rectangular microstrip antenna design for 5G broadband applications operating at 26 GHz is proposed [22–25]. This design featured an array and inset feed line contact, incorporating coupled slot feeding, array elements, and a ring to a rectangular patch antenna to boost gain and bandwidth, meeting the demands of 5G technology.

Ensuring that antennas meet specific performance parameters is critical for their effective operation in the desired frequency ranges. Microstrip antennas are favored for their com-

* Corresponding author: Chinnathambi Murugan (jaimurugan.c@gmail.com).

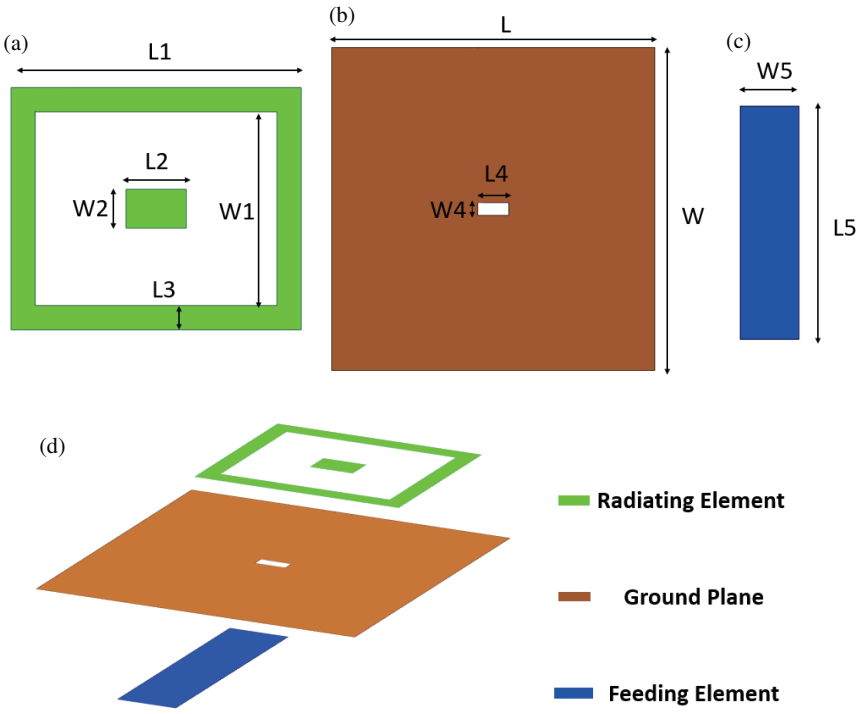

FIGURE 1. (a) Radiating patch. (b) Ground plane. (c) Feeding element. (d) Overall structure of the proposed antenna.

pact size and cost-effective manufacturing, making them well suited for high-frequency operations. They can also be easily printed and integrated onto the same board as the circuit [26]. This study introduces a dual-band antenna operating at 5.2–5.3 GHz and 5.9–6.1 GHz, with dimensions of 25 mm × 25 mm. It demonstrates a unique transition from monopole to broadside radiation and achieves a peak gain of 6.025 dBi. Printed on a 1.6 mm thick FR4 substrate, the compact design ensures practicality. Comprehensive testing shows excellent agreement between simulated and measured results, verifying the antenna's reliability. Its design offers adaptability in dual-band applications, enabling flexible and reliable signal reception across multiple frequencies, making it ideal for scenarios requiring robust performance.

The novelty of this study lies in the dual-band functionality and adaptable radiation patterns of the aperture-coupled slot-fed antenna. Unlike conventional designs, this antenna operates in two distinct frequency bands (5.2–5.3 GHz and 5.9–6.1 GHz) with unique pattern switching, offering monopole radiation at lower frequencies and a broadside pattern at higher frequencies. This dynamic pattern reconfiguration sets it apart, providing flexibility for diverse applications such as Wi-Fi (IEEE 802.11), 5G small cells, ITS, V2X communication, and satellite uplinks. Additionally, the compact structure, precise engineering on two FR4 substrates, and alignment of simulated and measured results emphasize its practicality and reliability for real-world deployments. The antenna's versatility in pattern adaptation within dual-band scenarios, along with its compact form and high performance, makes it a pioneering solution for environments requiring flexible and robust signal reception.

2. STRUCTURE OF SINGLE ELEMENT ANTENNA

The antenna specifications include operating frequencies of 5.25 and 6 GHz, maintaining a 50-ohm input impedance at the feeding point and achieving a minimum gain of 12 dB, as per the International Telecommunication Union-Telecommunication standard sector's reference. The selection of a rectangular microstrip patch antenna is based on its simplicity, low-profile design, and slot-feeding strategy aimed at maximizing bandwidth expansion and gain enhancement. The chosen substrate material has a dielectric constant of 4.4, with a substrate thickness of 3.2 mm. The feeder width is set at 0.86 mm. The overall structure consists of three layers: patch layer, ground plane layer, and feedline layer.

The designed single element is depicted in Figs. 1(a)–(d). Fig. 1(a) shows a top view of the structure, illustrating the composition of the antenna with a patch layer, a ground plane layer, and a feeding layer separated by a substrate material. The total substrate thickness is measured from the patch layer to the feeding layer. Fig. 1(b) displays the configuration of the ground plane. Fig. 1(c) illustrates the feeding structure. Fig. 1(d) presents an isometric view of the proposed aperture-coupled antenna. The methodologies outlined by Balanis [18] are utilized in various equations describing the geometry of the radiator, ground plane, feeding line, and slot structures. The calculation of a microstrip antenna's typical bandwidth (BW) often relies on the equation introduced in [19]. The theoretical perspective on fractional bandwidth is characterized as the ratio of the bandwidth to the resonant frequency.

$$\text{Fractional Bandwidth (\%)} = \frac{F_h - F_l}{F_r} \times 100\%.$$

Here, F_h and F_l denote the upper and lower frequencies of the antenna, respectively. These frequencies are extracted from the region where $S_{11} < -10$ dB.

3. FEEDING STRUCTURE

Antenna designers commonly employ coupled slot feeding technique to feed microstrip antennas. This method involves coupling the microstrip patch through a slot on the ground plane and offers several advantages over alternative feeding methods. It enhances bandwidth by introducing an additional degree of freedom through the slot, allowing tuning of the resonant frequency and achieving a broader impedance bandwidth. Additionally, it reduces insertion loss by providing a more efficient means of coupling energy from the feedline to the antenna. The coupled slot feeding technique also results in compact, low-profile antennas with polarization flexibility. Its seamless integration with other microwave components, such as filters, couplers, and amplifiers, makes it a favored choice among antenna designers. The given equation provides an approximation for the characteristic impedance of a strip feeding with a width denoted as $w0$, subject to the condition $w/h > 1$.

$$Z_{char} = \frac{120\mathrm{X}\pi}{\sqrt{\xi}_{eff}\left[\frac{w}{h} + 1.393 + 0.667\ln\left(\frac{w}{h} + 1.444\right)\right]}.$$

The optimal angular angle for the E-plane in coupled slot feeding is expressed by the following equation for a rectangular slot with dimensions L_s and W_s, where optimum directivity is attained within the sector angle ($0 \leq \theta \leq \theta$EH) for both E-plane and H-plane.

$$L_s = \frac{\lambda}{\sin\theta} \quad (E\text{-Plane}),$$

$$W_s = \frac{\lambda}{\sin\theta} \quad (H\text{-Plane})$$

The provided equation expresses the return loss, a measure indicating the power loss reflected from the load back toward the source resulting from impedance mismatch [20].

$$\text{Return Loss (dB)} = -S_{11}\ \text{dB}$$

Here, S_{11} is equivalent to the reflected coefficient Γ, representing the ratio between the incident and reflected waves.

$$S_{11} = \Gamma = \frac{b_1}{a_1}.$$

In this context, a_1 and b_1 correspond to the incidence and reflected waves, respectively.

$$S_{11}[\text{dB}] = 20\log 10(|\Gamma|).$$
$$S_{11}\,(\text{dB}) = 20\log\left(|\Gamma|\right).$$

Simulated S-parameters of the proposed antenna are illustrated in Figure 2, and it is observed that the antenna performes at 5.3 and 6.1 GHz with 10 dB impedance bandwidth. In the graphical representation depicted in Fig. 3(a), a notable observation reveals that the peak current concentration

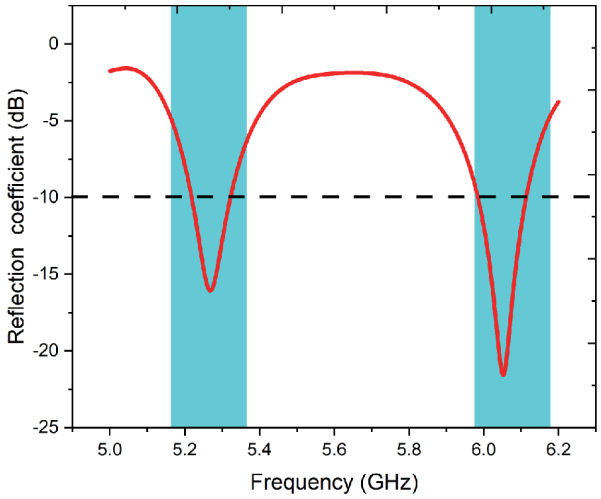

FIGURE 2. Simulated reflection coefficient.

prominently appears along the peripheries of the slot within the ground plane. Conversely, in a contrasting scenario illustrated in Fig. 3(b), the investigation demonstrates that the maximum current is not confined to specific locations but is instead distributed uniformly across the entire vicinity surrounding the slot. This uniform current distribution results in a radiation behavior consistent with a broadside pattern.

Figures 4(a) & (b) illustrate 3-D far-field radiation patterns of an antenna at two different frequencies, 5.3 GHz and 6.1 GHz, demonstrating monopole and broadside modes, respectively. At 5.3 GHz, the antenna operates in a monopole mode, exhibiting a characteristic doughnut-shaped radiation pattern with maximum radiation concentrated in the plane perpendicular to the antenna's axis (the X-Y plane), which is typical of monopole antennas. This is evident from the red regions representing the highest gain, while the reduced radiation along the Z-axis (blue regions) suggests weaker radiation in that direction. At 6.1 GHz, the antenna transitions into a broadside mode, where the radiation is primarily directed normal to the antenna surface, along the Z-axis. The broadside mode is commonly associated with higher directivity towards the broadside of the antenna, as indicated by the strong red and green regions along the Z-axis. This transition between monopole and broadside modes highlights the antenna's capability to switch radiation characteristics depending on the operating frequency, offering versatility for different applications. Consequently, the intricacies of the designed antenna's behavior unveil a noteworthy characteristic: A pattern diversity feature inherent in its dual-band frequency operation.

4. MEASURED RESULTS AND DISCUSSIONS

The proposed aperture-coupled slot-fed antenna prototype is meticulously presented in both its frontal and rear perspectives, depicted in Figs. 5(a) and (b), respectively. The antenna's performance is evaluated by measuring its reflection coefficient, using Keysight's vector network analyzer (VNA), and it is plotted in Figure 6 along with simulated results. A noteworthy observation emerges from the comparison between simulated and

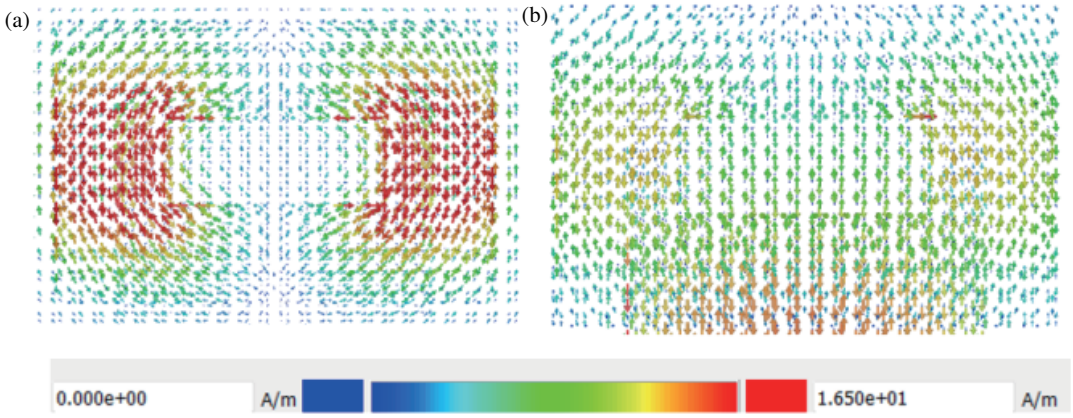

FIGURE 3. Simulated current distribution at (a) 5.3 GHz and (b) 6.1 GHz.

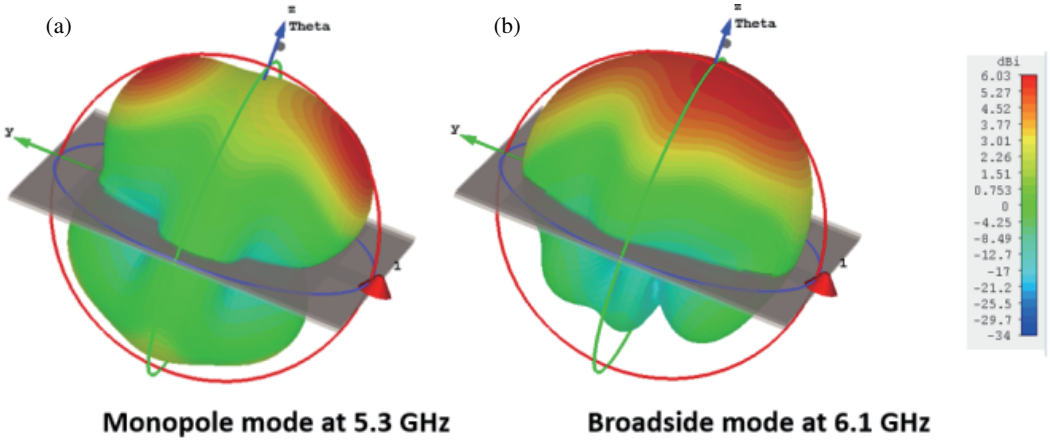

FIGURE 4. 3-D far-field pattern at (a) 5.3 GHz and (b) 6.1 GHz.

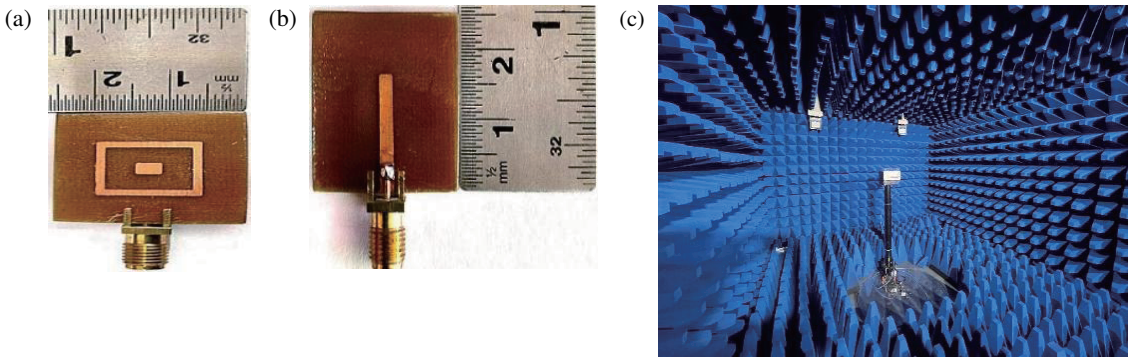

FIGURE 5. Fabricated prototype. (a) Front view. (b) Back view. (c) Measurement setup.

measured results, revealing a remarkable correlation between the two sets of data. This alignment underscores the accuracy and reliability of the antenna's simulated characteristics, affirming the fidelity of the design and its real-world performance.

The gain patterns at both extremes of each frequency are illustrated in Figs. 7 and 8. The antenna's behavior unfolds with distinct characteristics: a broadside pattern in the lower band and a monopole-like pattern in the upper band. This duality in radiation patterns across different frequencies of operation signifies the versatility and adaptability of the antenna design, making it well suited for diverse operational scenarios. The graphical representation in Figs. 7 and 8 serves as a visual testament to the antenna's ability to seamlessly transition between these distinctive radiation patterns, highlighting its efficacy across a range of frequencies.

The simulated and measured gains of the proposed antenna is illustrated in Fig. 9. The proposed antenna achieves the max-

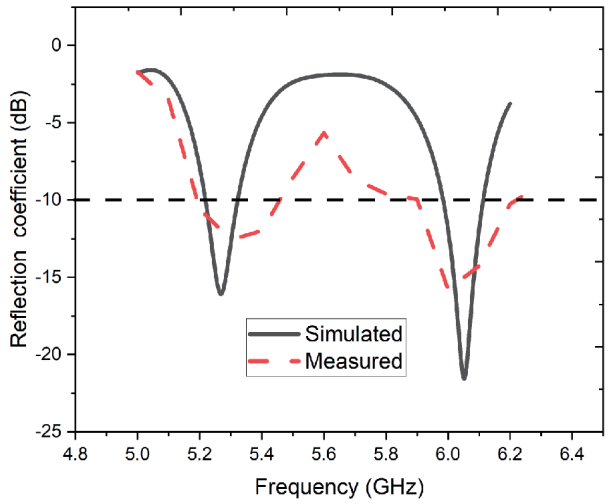

FIGURE 6. Simulated and measured reflection coefficients of the proposed antenna.

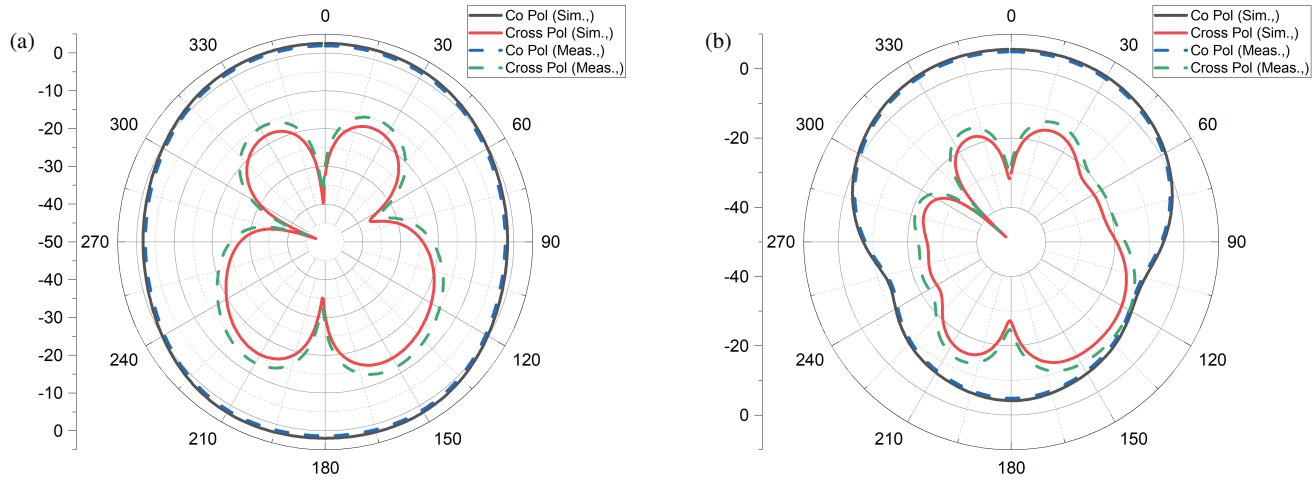

FIGURE 7. *E*-plane pattern at (a) 5.25 GHz, (b) 6.1 GHz.

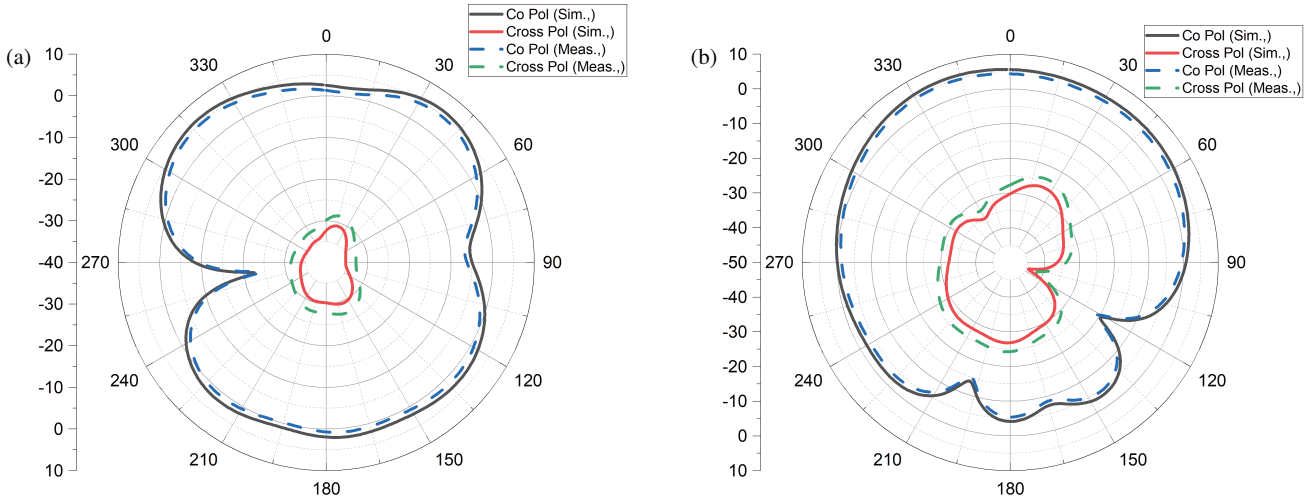

FIGURE 8. *H*-plane pattern at (a) 5.25 GHz, (b) 6.1 GHz.

TABLE 1. Comparison of the proposed antenna with literature.

Reference	Antenna type	Number of metallic layers	Fractional bandwidth	Dual-band covered
[21]	Patch	2	2%	No
[22]	Patch	2	4.8%	No
[23]	Patch	3	3.19%	No
[24]	Dipole	5	27%	No
[25]	Patch	1	NA	No
[26]	patch	3	5.4%	No
Proposed work	**Slotted patch**	**3**	**5% and 2.2%**	**Yes**

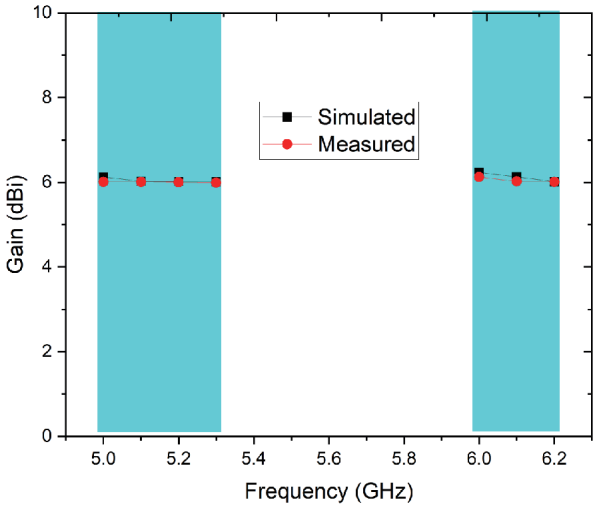

FIGURE 9. Simulated and measured gains of the proposed antenna.

imum gain of up to 6.03 dBi over both the bands of operation which is substantially sufficient for high gain wireless applications.

In an anechoic chamber, the gain of an antenna is measured by first setting up the test environment to eliminate external interferences and reflections. The antenna under test (AUT) is placed in the chamber, often on a rotating platform, allowing it to be oriented in various directions to measure the gain in both azimuth and elevation planes. A reference antenna with a known gain, such as a horn antenna, is used for calibration. A signal generator feeds the reference antenna, and the received signal strength is measured using a spectrum analyzer or receiver. The procedure involves first calibrating the chamber by measuring the reference antenna's signal strength, then replacing the reference with the test antenna and measuring the signal that it receives or radiates. The gain is calculated by comparing the received signal from the AUT with that from the reference antenna, adjusting for factors such as distance and frequency. This process ensures accurate measurement of the test antenna's directivity and power output in the chamber's controlled environment.

In comparison to existing works referenced in Table 1, the proposed aperture-coupled antenna offers several distinct advantages. Firstly, its unique design as a slotted patch antenna sets it apart from conventional patch and dipole antennas, potentially leading to improved performance in terms of radiation characteristics. Secondly, with three metallic layers, the proposed antenna matches the highest number of layers among the referenced works. This feature suggests the potential for enhanced performance and control over radiation properties. Moreover, with fractional bandwidths of 5% and 2.2%, the proposed antenna offers comparable or superior frequency coverage compared to existing works, ensuring versatility in accommodating different communication standards or frequency bands. Notably, the ability of the proposed antenna to cover dual bands further enhances its applicability, a feature not present in any of the referenced works. Overall, by combining these features, the proposed antenna demonstrates advancements over existing works, promising improved performance, versatility, and integration capabilities in various wireless communication systems

5. CONCLUSION

In summary, the development of a specialized aperture-coupled slot-fed antenna for dual-frequency bands, operating seamlessly within the 5.2–5.3 GHz and 5.9–6.1 GHz ranges, showcases its unique features. Its capability to emit monopole radiation at lower frequencies and transition to a broadside pattern at higher frequencies is a notable achievement. With a peak gain of 6.025 dBi within a compact 25 mm $\times$ 25 mm design, precisely printed on two 1.6 mm thick FR4 substrates, this antenna combines performance and practicality. Meticulous measurements of the constructed prototype validate its reliability and precision, showing a commendable alignment between simulated and measured outcomes. Its engineered adaptability caters to applications requiring diverse patterns in dual-band scenarios, allowing for adaptive signal reception. This adaptability positions the antenna favorably for scenarios requiring robust performance across multiple frequency ranges. The antenna's ability to offer expanded pattern variations holds significant promise in fields where flexible and robust signal reception is indispensable.

REFERENCES

[1] Support 5G, *ITU News Magazine*, Nov. 2019.

[2] Andrews, J. G., S. Buzzi, W. Choi, S. V. Hanly, A. Lozano, A. C. K. Soong, and J. C. Zhang, "What will 5g be?" *IEEE Journal on Selected Areas in Communications*, Vol. 32, No. 6, 1065–1082, Jun. 2014.

[3] Agiwal, M., A. Roy, and N. Saxena, "Next generation 5G wireless networks: A comprehensive survey," *IEEE Communications Surveys & Tutorials*, Vol. 18, No. 3, 1617–1655, 2016.

[4] International Telecommunication Union, "Additional frequency bands identified to," Jun. 2014.

[5] Series, M., "IMT Vision — Framework and overall objectives of the future development of IMT for 2020 and beyond," *Recommendation ITU*, Vol. 2083, 1–21, 2015.

[6] Thakur, V., N. Jaglan, and S. D. Gupta, "A review on antenna design for 5G applications," in *2020 6th International Conference on Signal Processing and Communication (ICSC)*, 266–271, Noida, India, 2020.

[7] Dewar, C. and D. Warren, "Understanding 5G - Perspectives on future technological advancements in mobile," *GSMA Intelligence*, 1–26, 2014.

[8] Chen, S. and J. Zhao, "The requirements, challenges, and technologies for 5g of terrestrial mobile telecommunication," *IEEE Communications Magazine*, Vol. 52, No. 5, 36–43, May 2014.

[9] Dwivedi, S., "Effect of thickness of substrate on antenna design for advance communication," in *2017 7th International Conference on Cloud Computing, Data Science & Engineering — Confluence*, 770–774, Noida, India, Jan. 2017.

[10] Kedze, K. E., H. Wang, Y. B. Park, and I. Park, "Substrate dielectric constant effects on the performances of a metasurface-based circularly polarized microstrip patch antenna," *International Journal of Antennas and Propagation*, Vol. 2022, No. 1, 3026677, Sep. 2022.

[11] Pratiwi, A. R., E. Setijadi, and G. Hendrantoro, "Design of two-elements subarray with parasitic patch for 5G application," in *2020 International Seminar on Intelligent Technology and Its Applications (ISITIA)*, 311–316, 2020.

[12] Amillia, F., E. Setijadi, and G. Hendrantoro, "The effect of parasitic patches addition on bandwidth enhancement and mutual coupling in 2×2 sub-arrays," *IEEE Access*, Vol. 10, 72 057–72 064, 2022.

[13] Srivastava, H., A. Singh, A. Rajeev, and U. Tiwari, "Bandwidth and gain enhancement of rectangular microstrip patch antenna (RMPA) using slotted array technique," *Wireless Personal Communications*, Vol. 114, No. 1, 699–709, 2020.

[14] Faeghi, P., C. Ghobadi, J. Nourinia, and B. Virdee, "Nanoparticle-coated Vivaldi antenna array for gain enhancement," *Applied Physics A*, Vol. 129, No. 3, 217, 2023.

[15] Koul, S. K. and G. S. Karthikeya, "Feeding techniques for mmwave antennas," in *Antenna Architectures for Future Wireless Devices*, 207–229, Springer, 2021.

[16] Ulfah, M. M., P. Janpugdee, and D. Torrungrueng, "Feeding effects to gain enhancement of microstrip antennas with partially reflective surfaces," in *2022 International Symposium on Antennas and Propagation (ISAP)*, 435–436, Sydney, Australia, Oct. 2022.

[17] Ghenjeti, S., R. Barrak, and S. Hamouda, "High gain and compact microstrip patch antenna array design for 26 GHz broadband wireless systems," in *2023 IEEE Symposium on Computers and Communications (ISCC)*, 932–937, Gammarth, Tunisia, Jul. 2023.

[18] Balanis, C. A., *Antenna Theory: Analysis and Design*, John Wiley & Sons, 2016.

[19] Volakis, J. L. and J. L. Volakis, *Antenna Engineering Handbook*, McGraw-Hill, 2007.

[20] Huang, Y., *Antennas: From Theory to Practice*, John Wiley & Sons, 2008.

[21] Yang, W., S. Chen, Q. Xue, W. Che, G. Shen, and W. Feng, "Novel filtering method based on metasurface antenna and its application for wideband high-gain filtering antenna with low profile," *IEEE Transactions on Antennas and Propagation*, Vol. 67, No. 3, 1535–1544, Mar. 2019.

[22] Bayatpur, F. and K. Sarabandi, "Miniaturized FSS and patch antenna array coupling for angle-independent, high-order spatial filtering," *IEEE Microwave and Wireless Components Letters*, Vol. 20, No. 2, 79–81, Feb. 2010.

[23] Bayatpur, F. and K. Sarabandi, "A metamaterial-based spatial filter for phased-array applications," in *2009 IEEE Antennas and Propagation Society International Symposium*, 1–4, North Charleston, SC, USA, Jun. 2009.

[24] Yepes, C., D. Cavallo, E. Gandini, S. Monni, A. Neto, and F. E. V. Vliet, "Angularly stable frequency selective surface combined with a wide-scan phased array," *IEEE Transactions on Antennas and Propagation*, Vol. 66, No. 2, 1046–1051, Feb. 2018.

[25] Hong, Y.-P., I.-J. Hwang, D.-J. Yun, D.-J. Lee, and I.-H. Lee, "Design of single-layer metasurface filter by conformational space annealing algorithm for 5G mm-Wave communications," *IEEE Access*, Vol. 9, 29 764–29 774, 2021.

[26] Li, Y., X. Nie, X. Yang, C. Liu, X. Lin, and K. Huang, "An aperture-coupled-cross-resonator FSS based spatial filtering patch antenna array," *IEEE Access*, Vol. 12, 5672–5683, 2024.